




## Article

# Sanded Wheel–Rail Contacts: Experiments on Sand Crushing Behaviour

Bettina Suhr <sup>1,\*</sup> , William A. Skipper <sup>2</sup> , Roger Lewis <sup>2</sup>  and Klaus Six <sup>1</sup>

<sup>1</sup> Virtual Vehicle Research GmbH, Inffeldgasse 21a, 8010 Graz, Austria

<sup>2</sup> Department of Mechanical Engineering, The University of Sheffield, Mappin Street, Sheffield S1 3JD, UK

\* Correspondence: bettina.suhr@v2c2.at

**Abstract:** In railway operation, the sanding process is used to overcome low adhesion conditions in the wheel–rail contact. In the literature, previously conducted research has been experimental, e.g., measuring adhesion coefficients (ACs) under different contact conditions (dry, wet, ...) or applying different sands. Under dry conditions, sanding can reduce measured ACs, while under wet conditions different types of rail sand can leave ACs unchanged or increase adhesion. Despite active research, the physical mechanisms causing the change in ACs under sanded conditions are still poorly understood. A possible remedy is the development of advanced models of sanding including local effects. As a basis for such a model, this study presents experimental results concerning single grain crushing behaviour of two types of rail sand under dry and wet contact conditions. Firstly, initial breakage behaviour is investigated with focus on the particle fragments' size and spread as only fragments within the running band are available to influence the AC during roll-over. Secondly, single grain crushing tests are conducted under realistic wheel–rail load showing the formation of solidified clusters of sand fragments, as well as their size and thickness. This information is important for understanding mechanisms and for future physics-based modelling of the sanding process in wheel–rail contacts.

**Keywords:** wheel–rail contact; low adhesion; sanding; single grain crushing tests



**Citation:** Suhr, B.; Skipper, W.A.; Lewis, R.; Six, K. Sanded Wheel–Rail Contacts: Experiments on Sand Crushing Behaviour. *Lubricants* **2023**, *11*, 38. <https://doi.org/10.3390/lubricants11020038>

Received: 16 December 2022

Revised: 12 January 2023

Accepted: 13 January 2023

Published: 20 January 2023



**Copyright:** © 2023 by the authors. Licensee MDPI, Basel, Switzerland. This article is an open access article distributed under the terms and conditions of the Creative Commons Attribution (CC BY) license (<https://creativecommons.org/licenses/by/4.0/>).

## 1. Introduction

In railway operation, the contact between wheel and rail is determined by complex tribological processes. Extremely high contact pressures and tangential stresses, caused for example by traction or braking, result in severe plastic deformation of the near-surface layers [1–7]. This influences damage and wear behaviour and the developing wheel–rail roughness affecting the transferable tangential force between wheel and rail. The tangential force is limited by the maximal adhesion coefficient (AC), which is around 0.35 or higher for dry conditions [8,9]. Between wheel and rail, third body layers (3BLs) can be embedded, such as liquids (e.g., water), solids (e.g., wear particles), or combinations thereof. Some of these 3BLs can cause low adhesion conditions with ACs below 0.1 [10–13]. Such low adhesion conditions influence the traction and braking performance of railway vehicles in service. In the worst case, they can cause safety issues [14,15]. Typical causes for low adhesion conditions are damp (wet) contact conditions [16] ('wet rail' phenomenon) or when the rail surface is contaminated with leaves [14,17].

The application of sand has been used for many years to overcome low adhesion conditions in the wheel–rail contact. Figure 1 shows the process divided into three phases. In phase I, the particles are applied: some are expelled and some are entrained into the contact. In phase II, particles are in the wheel–rail contact and influence the adhesion. Finally, in phase III particles leave the contact and some of them remain on wheel and rail.

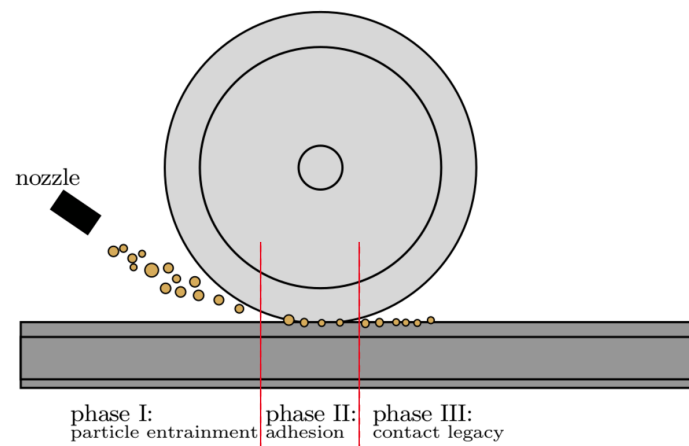


**Figure 1.** Phases during wheel–rail contact sanding.

Under low adhesion conditions, sanding generally increases the maximal AC between wheel and rail, but it can also lead to increased damage on both wheel and rail [18,19]. Wheel–rail sanding is a field of active research, where the adhesion increasing aspect is more extensively investigated [20] than the damage or isolation aspects [21]. Research is conducted with both field testing and lab experiments, e.g., twin-disc tests [22–25], linear full-scale rigs [26], or high pressure torsion (HPT) test rigs [27,28]. Indentations were measured on both wheel and rail as well as wheel–rail ACs under different contact conditions (dry, wet, or different kinds of contamination) but also with different types of sand [27] or different amounts of sand being applied [25]. In static loading tests [19], indentations were observed mainly on the wheel. Large indents could be caused by large particles being embedded into the surface prior to crushing or because the grain fractures into larger bits, which remain together. Smaller indents were possibly formed by crushed particles. These different mechanisms could lead to differences in the change of roughness caused by sanding. Large indents of embedded sand particles were also found in twin-disc tests under wet conditions [25] together with small amounts of spalling and pits. Under dry conditions, sanding can have little effect or even reduce measured ACs [22,27,28]. In contrast, under wet conditions different types of rail sand can leave ACs unchanged or increase adhesion, where some sands restore adhesion to nearly dry conditions [25,27,28]. The described behaviour can be seen in Figure 2, where measured ACs from HPT tests under dry and wet conditions are shown, using two different types of sand.

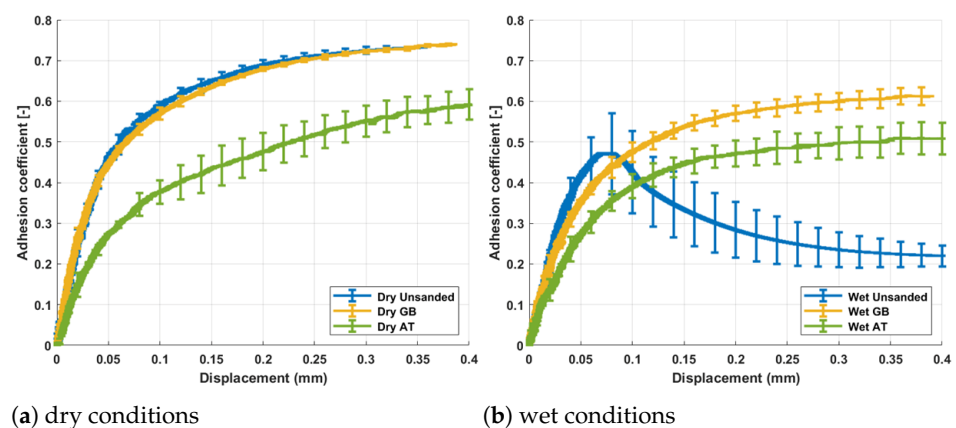


**Figure 2.** Influence of sanding on adhesion coefficient under dry and wet conditions in a HPT test. Two different types of sand were applied, for more details see [28].

Despite the active research in this field, the physical mechanisms causing the change in ACs under sanded conditions are still poorly understood. Sand grains will partially

crush when entering the contact, causing plastic deformations on wheel and rail surfaces (i.e., change of roughness). The amount of sand in the contact determines whether the metal surfaces are (partially) separated or not, allowing for different mechanisms of load transfer, see Figure 3. Under high loads, sand fragments solidify and could form clusters, which indent into wheel and rail surfaces (affecting roughness) and cause form closure effects. Adhesion could also be increased via form closure effects caused by sand grains directly penetrating into wheel–rail surfaces, or the sand powder solidifies and partially covers the rough wheel–rail surfaces, increasing the effective contact area between sand and steel and thereby the AC. The role of water in wet contacts is also unclear. This mentioned lack of understanding is caused by the fact that current experimental abilities do not allow for any monitoring of the aforementioned mechanisms in the contact zone during roll-over.

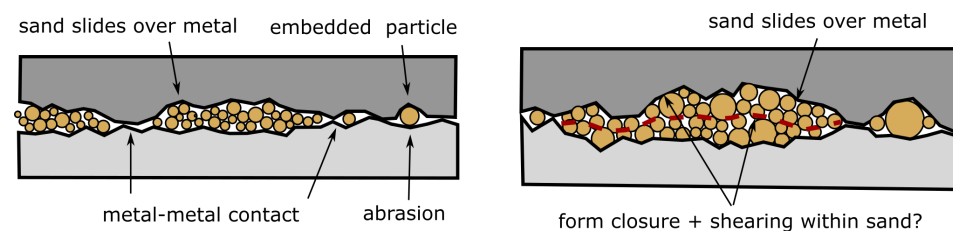


**Figure 3.** Possible mechanisms for increasing adhesion via sanding.

Models predicting the normal and tangential contact stresses (forces) in the wheel–rail interface are mostly based on classical theory [29–41]. Such models will not help with gaining new insights about physical phenomena occurring in the contact when sand is introduced. The only possibility to account for the influence of sand in these models is to change the coefficient of friction. Beside models based on classical theory, extended models can be found in the literature, see [29,41] for an overview. For example, in [9,10,42,43] models are presented, which account for the influence of solid 3BLs on the adhesion characteristic. However, these models assume a continuous 3BL across the contact and thus spread local effects (e.g., resulting from sand grains) within the contact region. Furthermore, the change of roughness due to local plasticity effects cannot be described. In [17], the approach from [9,10] and the model from [8] are combined. However, the model represents a semi-physical approach not explicitly accounting for the physical effects occurring in the contact zone mentioned previously. Thus, the impact of sand under low adhesion conditions cannot be described with this methodology either.

To summarise, although the positive effect of sand is well known and experimentally proven, the physics behind this improvement are not yet fully understood (effects occurring in the contact patch during roll-over of sand particles cannot be observed). Furthermore, models taking into account local effects are not available. Such models in combination with experiments are important for a better understanding of the physics occurring in sanded contacts. This could be particularly useful for aims as, e.g., reducing the amount of sand necessary to increase adhesion and thus reducing/avoiding damage due to sanding.

This study is part of a research project where sanded contacts are experimentally investigated in detail, and advanced models are to be developed to better understand the phenomena responsible for the positive effect of sand on adhesion in phase II, see Figure 3. The experimental work on single sand grains aims for a better understanding of the material behaviour and should also generate the necessary information for model development and parameterisation.

In this paper, two types of rail sand were investigated. Single grain crushing tests were conducted under dry and wet contact conditions to investigate the initial breakage behaviour. In the sanding process, the first fracture will take place several centimetres in front of the contact patch due to the narrowing gap between wheel and rail. Some of the resulting fragments are expelled from the running band (and are thus not active any more), while others stay inside and be crushed again. Therefore, focus in the conducted tests were

on the particle fragments' size and spread after the first crushing. Furthermore, a Weibull statistic was fitted to the measured data.

In a second step, single grain crushing tests were conducted under a realistic wheel–rail load of 900 MPa, this included the initial crushing and subsequent further crushing of the fragments remaining in the contact area. These tests aimed to provide information about the condition of the sand after it had been fully loaded in a vertical direction: the possible formation of solidified clusters of sand fragments, as well as their size and thickness. This information is important for understanding mechanisms and for physics-based modelling of the sanding process in wheel–rail contacts. Finally, Scanning Electron Microscope (SEM) images were taken from some of the formed sand clusters after full loading to gain information about the surface structure and to see if they were composed of connected smaller fragments.

## 2. Single Grain Crushing: First Breakage

These tests investigate the state of sand grain fragments after the first breakage event. The analysis of fragments' size and spread shows how much of the material is available (after first breakage) in the area of an conceptual wheel–rail contact. This information is important for understanding possible mechanisms of the influence of sanding on the adhesion coefficient.

### 2.1. Materials and Methods

Rail sands from Great Britain (GB) and Austria (AT) were used in this study. Both sands were riffled down to 100 g to ensure a representative sample [44], each sample was then subjected to sieve analysis to determine the average particle size [45]. The average size of GB was 1.30 mm and AT was 0.98 mm. For all particle crushing tests particles of approximately average size were desired. Therefore, particles passing through a sieve aperture of 1.4 mm and settling on a sieve with an aperture of 1.18 mm were used for GB tests; for AT tests these respective sieve apertures were 1.18 mm and 0.6 mm.

Single particle crushing tests till first fracture were performed on a Bruker (Bruker, Coventry, West Midlands, UK.) universal mechanical tester (UMT) using a 1000 N load cell with a resolution of 50 mN. The set-up of this test is shown in Figure 4. The first fracture was defined by a sudden, large drop in measured load. An example of a measured path–force curve is shown in Figure 5, where the peak load before first fracture is marked. The tests were performed in displacement control with a speed of 0.05 mm/s. Both top and bottom platens had contacting faces with a  $50 \times 50 \text{ mm}^2$  contact area, with the bottom platen being made from EN24 grade steel and the top platen from EN5.

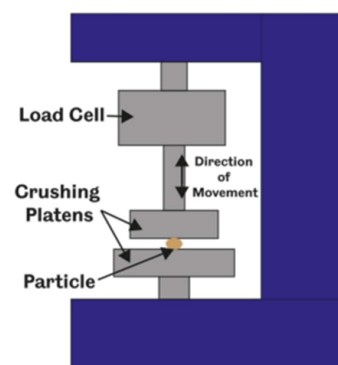


**Figure 4.** Test set-up for single particle crushing tests in the UMT test rig.



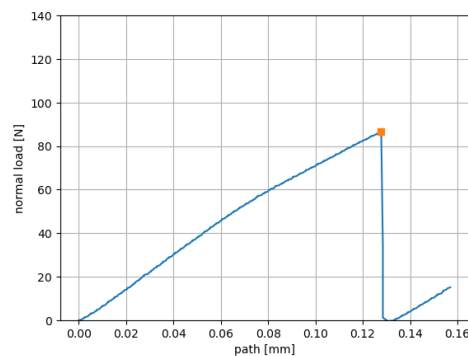


**Figure 5.** Examples of a measured path–force curve from a single crushing test, with the particle breakage force shown as orange square symbol.

Tests were conducted with GB sand and AT sand, respectively, in dry and wet conditions. Here, wet conditions were created by pipetting 10 or 20  $\mu\text{L}$  of distilled water onto the particle. A total of 30 tests were performed for each condition. However, some tests had to be excluded from further analysis due to different problems occurring. In some tests, grains showed successively small fractures without a clear peak force, this was more often the case for AT sand. In a few tests, no clear grain breakage occurred despite a high loading path. For GB sand, there were several cases, where the path–force curve showed a yielding-like behaviour, where unusually high loading paths were reached together with very high breakage forces. Possible reasons could be an indenting of the grain in the steel plates. This behaviour was seen only for GB sand, which has a higher Young’s modulus than AT sand [28]. For the fitting of the Weibull statistics, 24 tests were used for GB sand in both dry and wet conditions. For AT sand, 24 tests were used for dry conditions and 25 for wet conditions. For the analysis of the fragments’ spreading a few further tests had to be excluded, where the test did not stop before a second severe breakage had taken place. For this analysis, 21 tests were used for GB sand under dry conditions and 23 tests under wet conditions. For AT sands, 23 tests each were analysed under dry and wet conditions.

Each particle was weighed before crushing and the fragments remaining on the platens were weighed after crushing to determine the amount of material expelled from the contact.

Before and after each test, photos were taken, see Figure 6. To be able to measure the initial particle’s area and the fragments’ area and position, these photos were segmented using the Fiji (Fiji: version 2.35.) [46] and Gimp (Gimp: version 2.10.22.) [47] software. In Fiji the photos were converted to black and white (setting 8 bit format) and then a manual threshold selection was applied. As the sand grains differed in their colour and brightness, a manual correction step was necessary using Gimp, which clearly introduced some impreciseness to the process. An example of the segmented photo after crushing can be seen in the right part of Figure 6. After the segmentation step, the Fiji software was applied using the “Analyze Particles” function to calculate the particle/fragments’ area, position, diameter, and other shape descriptors. With the segmented photo after crushing, for each fragment the distance from the centre of the initial grain was calculated.

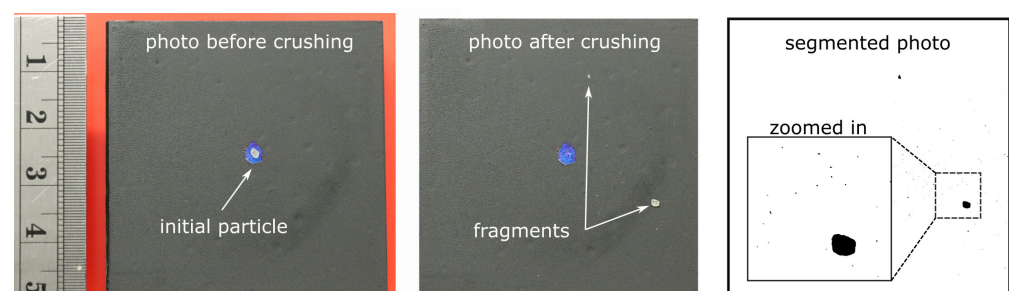


**Figure 6.** Examples for photos taken and post-processing.

## 2.2. Results: Analysis of Fragment's Size and Spread

In the following analysis, no distinction is made between tests under wet conditions using 10  $\mu\text{L}$  or 20  $\mu\text{L}$  of water, as for both cases the results were very similar.

In Figure 7, histograms of the fragments' distance from the centre and the fragments' area can be seen for both GB and AT sand under dry and wet conditions. For GB sand under dry conditions, the grain's fragments spread out with a slow decrease until 35 mm distance. In contrast, under wet conditions more than 96% of the GB sand's fragments have a distance smaller than 5 mm.

For AT sand under dry conditions, 68% of all fragments have a distance from the centre less than 5 mm. The probability of fragments at higher distances decays faster and is almost 0 for values higher than 25 mm. This is a clear difference to the behaviour of GB sand under dry conditions. AT sand under wet conditions shows the least spreading of all cases investigated: 98% of the fragments have a distance less than 5 mm.

In Figure 7c,d, histograms of the fragments' area are shown. Here, the results for both types of sand and for dry and wet contact conditions are similar. The vast majority of fragments are smaller than 0.1 mm (size of the histograms first bin) and only few larger particles exist.

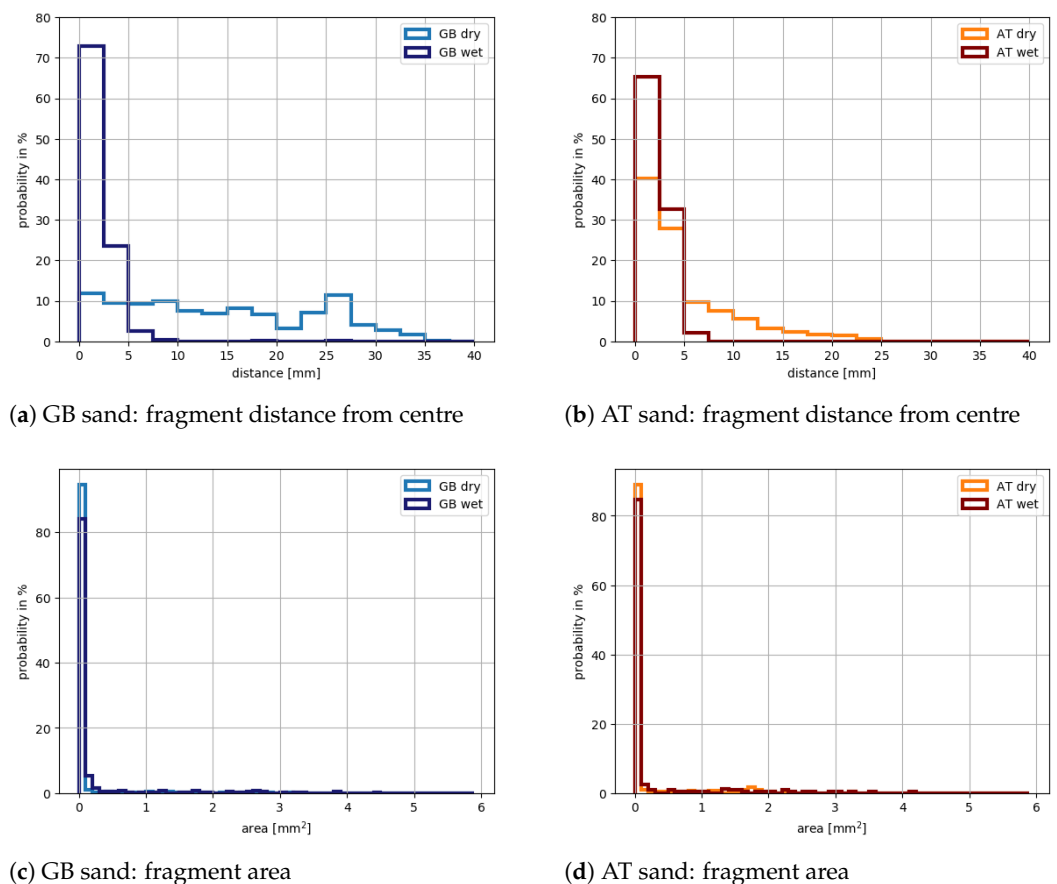


**Figure 7.** Distance and area for GB and AT sands.

Thinking of the application of wheel–rail sanding, it is of interest to ask how much of the mass of the initial grain would stay within a radius of 5 mm: radius of a conceptual wheel–rail contact patch. This radius corresponds to a typical running band width when the tread of a wheel is in contact with the rail head. Experimental results using a full-scale test rig can be found in [48]. From the post-processing of the crushing tests, the fragments' area and distance can be related. Figure 8 shows cumulative histograms, where the fragment distance is weighted by its area divided by the sum of all fragments. The area of the conceptual wheel–rail contact is shown as grey box. For GB sand, the contact condition

makes a big difference: under dry conditions 68% of the fragments' area stay within the conceptual wheel–rail contact, while it is 98% under wet conditions. This influence of the contact condition is less pronounced for AT sand: Even under dry conditions 93% of the fragments' area stays within the conceptual wheel rail contact and under wet conditions it is 100%.

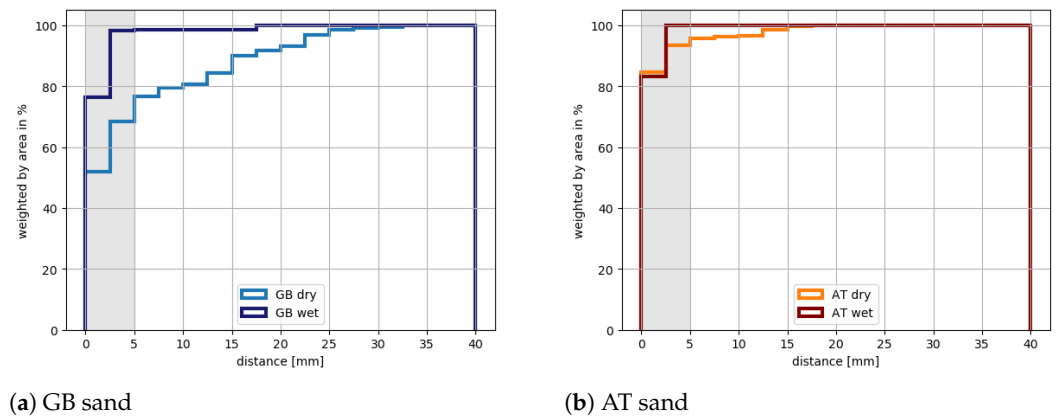


**Figure 8.** Distance weighted by area for GB and AT sands. The area of an conceptual wheel–rail contact is shaded in grey.

The previous analysis took into account the fragments which remained on the lower plate (sized 5 cm × 5 cm) of the testing device. To check if any fragments were expelled from this lower plate, the weight of the initial grain was recorded, as well as the weight of the fragments remaining on the lower plate. In some cases, fragments stuck to the upper plate of the testing device. In the check for mass loss, these fragments' weight was added to the fragments' weight from the lower plate. Figure 9 shows box plots of the mass loss for GB and AT sands for both contact conditions. For GB sand under dry conditions, the mass loss ranged up to 10% while there were four outliers reaching up to 66%. Under wet conditions on GB sand, there were three outliers with a mass loss between 25% and 33%, while in all other cases the mass loss was below 3%. For AT sand under both dry and wet conditions the mass loss was below 7%, with the exception of four tests under dry conditions, which ranged between 15% and 42% of mass loss. It is consistent with the fragments' spread behaviour that GB sand under dry conditions has a higher mass loss than under wet conditions. The results for AT sand are similar for dry and wet conditions, which is also in accordance with their spread behaviour. Comparing mass loss results between GB and AT sand, AT sand shows higher values than expected from the spread behaviour. The observed mass loss was often close to the accuracy of the scale used for measuring and as AT sand grains are smaller than GB sand grains. This could be a possible explanation.

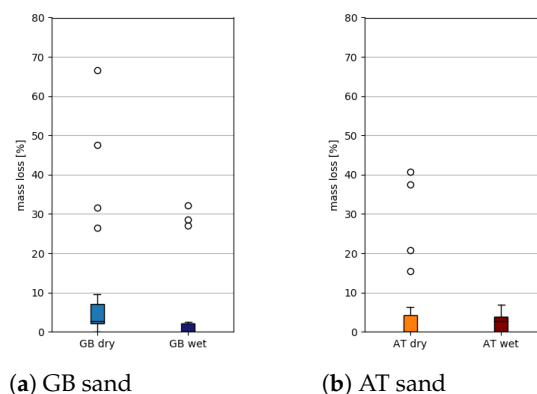


**Figure 9.** Mass loss after grain crushing test for GB and AT sands.

### 2.3. Results: Fitting of Weibull Statistics

For later use in modelling of particle breakage, the Weibull statistics will be fitted to the measured breakage force/probability of survival of GB and AT sand. In this section, no distinction between dry and wet contact condition will be made, as it is assumed that the contact condition does not influence the breakage force.

The particle breakage force is defined as the highest force before a clear drop in the force can be seen, compare in Figure 5 the orange square symbol. Denoting the force at particle breakage with  $F_b$  allows the calculation of the stress at breakage [49–51]

$$\sigma_b = \frac{F_b}{d^2}, \quad (1)$$

where  $d$  denotes the grain's diameter. The survival probability of a grain of diameter  $d$  under stress  $\sigma$  is described using Weibull statistics [49–52]:

$$P_s(d) = \exp \left[ - \left( \frac{d}{d_0} \right)^3 \left( \frac{\sigma}{\sigma_0} \right)^m \right], \quad (2)$$

where  $d_0$  is the reference diameter,  $m$  is the Weibull modulus, and  $\sigma_0$  is the characteristic stress such that a particle of size  $d_0$  has 37% survival probability. The reference diameter is the median of the used particle diameters, shown in Figure 10a. It can be seen that  $d_0$  is clearly larger for GB sand compared to AT sand. Note that the values shown are higher than the sieve sizes mentioned in the experiment description: thin particles may pass the sieve aperture diagonally and in image analysis a larger diameter can be measured depending on the orientation of the particle. The breakage forces are shown in Figure 10b, and for GB sand they reach up to 103 N, while for AT sand they are well below 65 N. Interestingly, the breakage stresses are mostly in the same range for both types of sand, compare Figure 10c.

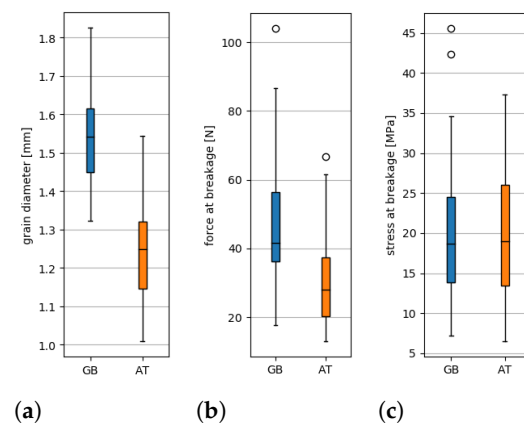


**Figure 10.** Grain diameter, force, and stress at breakage for GB and AT sands. (a) Diameter; (b) force at breakage; (c) stress at breakage.

Using the calculated stresses and assigning survival probabilities, the Weibull statistics is fitted to the data [50]. A comparison of measured values from the experiment and the fitted Weibull statistics is shown in Figure 11 for both types of sand. The parameters of the fitted Weibull statistics are given in Table 1. The results are surprisingly similar for both types of sand, considering the differences found in the analysis of fragment's spread.

**Table 1.** Parameters of the fitted Weibull statistics for both GB and AT sand.

Sand Type	$d_0$ (mm)	$\sigma_0$ (MPa)	$m$ (-)
GB	1.54	22.74	2.85
AT	1.25	22.49	2.72

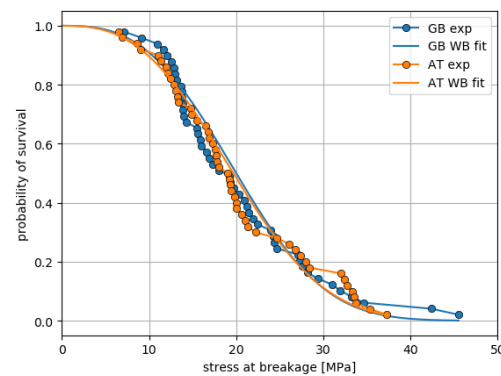


**Figure 11.** Fitted Weibull statistics.

### 3. Single Grain Crushing: High Loading

These tests aim to provide information about the condition of the sand after it has been fully loaded in the vertical direction. There is the possible formation of solidified clusters of sand fragments and their size and thickness are of interest. This information is important for understanding and physics-based modelling of the sanding process in wheel–rail contacts.

#### 3.1. Materials and Methods

Single particle crushing tests under realistic wheel–rail contact pressures were carried out using a Denison Mayes (Denison Mayes, Leeds, West Yorkshire, UK.) hydraulic test frame. The set-up of this experiment is included in Figure 12. The bottom platen had an area of  $50 \times 50 \text{ mm}^2$  whereas the top platen had a circular area with a 11 mm diameter. This meant the applied contact pressure was 900 MPa at the load capacity of the rig (90 kN). Both platens were made of hardened O1 tool steel to minimise the amount of plastic deformation of the surfaces upon crushing the particle. For both GB sand and AT sand, 5 tests were conducted under dry and wet conditions each, totalling 20 tests. For wet conditions, 20  $\mu\text{L}$  of distilled water were applied by pipette.

Mass measurements and photos were taken for each particle in the same manner as was performed for the UMT testing. Moreover, a non-contact imaging and measuring tool named Alicona (Bruker, Market Harborough, Leicestershire, UK.) InfiniteFocus SL was used to take high resolution 3D scans of the crushed grain on the lower plate after the test. These scans had a vertical resolution of 500 nm.

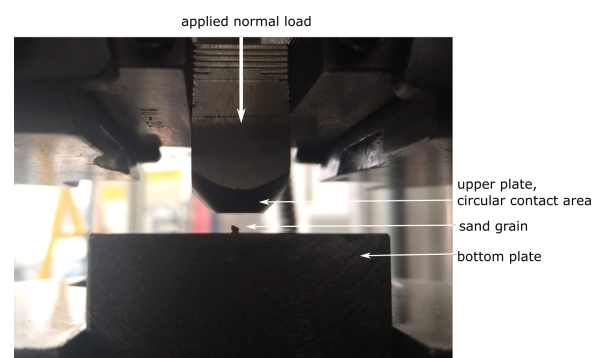


**Figure 12.** Test set-up for single particle crushing tests under realistic wheel–rail contact pressures.

SEM samples were prepared from the remains of the particles crushed under high load by removing the fragments from the crushing surface and mounting them onto stubs. SEM imaging was conducted using an FEI (FEI, Hillsboro, OR, USA.) Nova NanoSEM 450 with an Everhart–Thornley Detector. Imaging voltage was 5 kV with a spot size of 3 and a working distance of 2.5–3.5 mm.



### 3.2. Results: Fragment Spreading under High Loading

During the tests, the sand grains fractured repeatedly, with varying amounts of fragments being expelled from the contact. However, in almost all tests the formation of clusters of solidified sand fragments was seen. Their size varied for both types of sand and for dry/wet contact condition.

GB sand under dry conditions showed a high variation in the amount of fragments, which stayed within the contact area. From the five conducted tests, in three tests several small clusters formed. An example can be seen in Figure 13a, where the marked cluster has a side length of about 1 mm. The corresponding Alicona scan, Figure 13b, shows heights between 40  $\mu\text{m}$  and 70  $\mu\text{m}$ . In one test, nearly all fragments were expelled from the contact, while in another test a large cluster of side length 3.8 mm formed, see Figure 13c. This cluster had a height of 40  $\mu\text{m}$  at the edges and 140  $\mu\text{m}$  at its centre in the Alicona scan, see Figure 13d. The observed behaviour, including a high spreading of fragments, is in accordance with the results from the first breakage test.

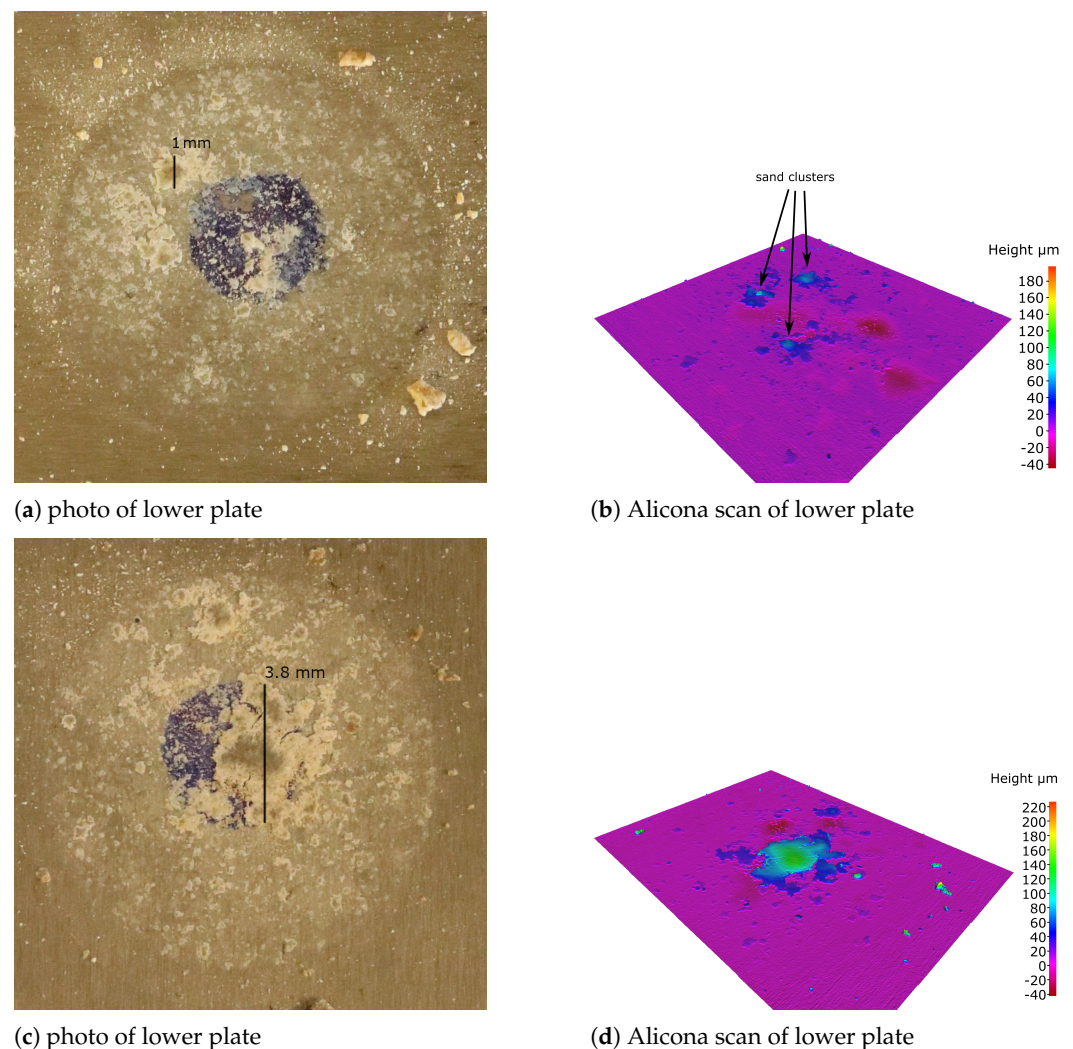


**Figure 13.** Example result for high load testing of GB sand under dry conditions.

The corresponding tests for AT sand under dry conditions showed larger sized clusters of solidified sand fragments in 4 of 5 tests. A typical result of the high load tests can be seen in Figure 14. This cluster has side length of about 3 mm and showed a height of 70  $\mu\text{m}$  at the edges and 140  $\mu\text{m}$  at its centre in the Alicona scan. In one test, several smaller clusters formed. These results are in accordance with the low amount of spreading of AT sand seen in the first breakage testing.



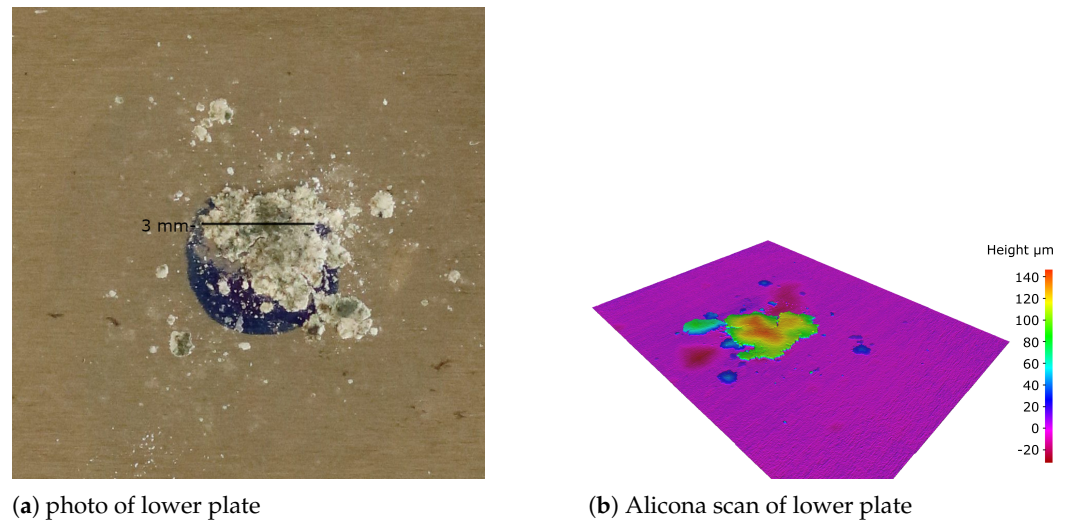


**Figure 14.** Example result for high load testing of AT sand under dry conditions.

Under a wet condition, both types of sand showed typically only one big cluster of solidified sand powder, see Figures 15 and 16. This is again in agreement with the initial breakage results presented, where the least spread of fragments was seen under wet conditions for both types of sand. The cluster of GB sand shown in Figure 15 had a side length of 4.4 mm and a height between 100  $\mu\text{m}$  and 220  $\mu\text{m}$ . In contrast, the cluster of AT sand shown in Figure 16 was much smaller with a side length of about 3 mm and heights between 60  $\mu\text{m}$  and 160  $\mu\text{m}$ . For both types of sand, one test existed, where the sand fragments seemed to have drifted in the applied water drop and no cluster was formed. In this study, no detailed analysis of the formed cluster's shape is conducted. Because of the described variations in the results and because of the low number of conducted high loading tests, no reliable conclusions could be drawn from such an analysis.

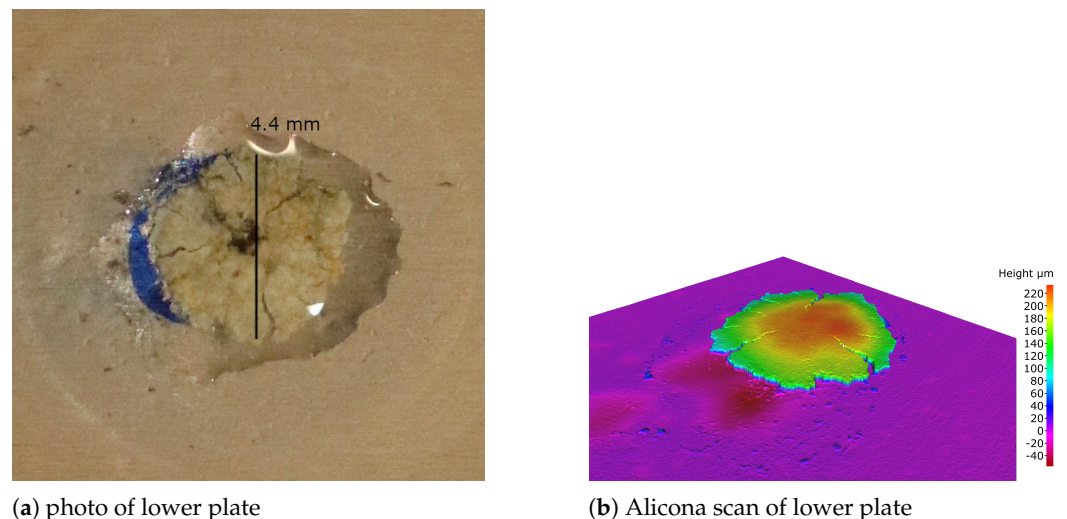


**Figure 15.** Example result for high load testing of GB sand under wet conditions.

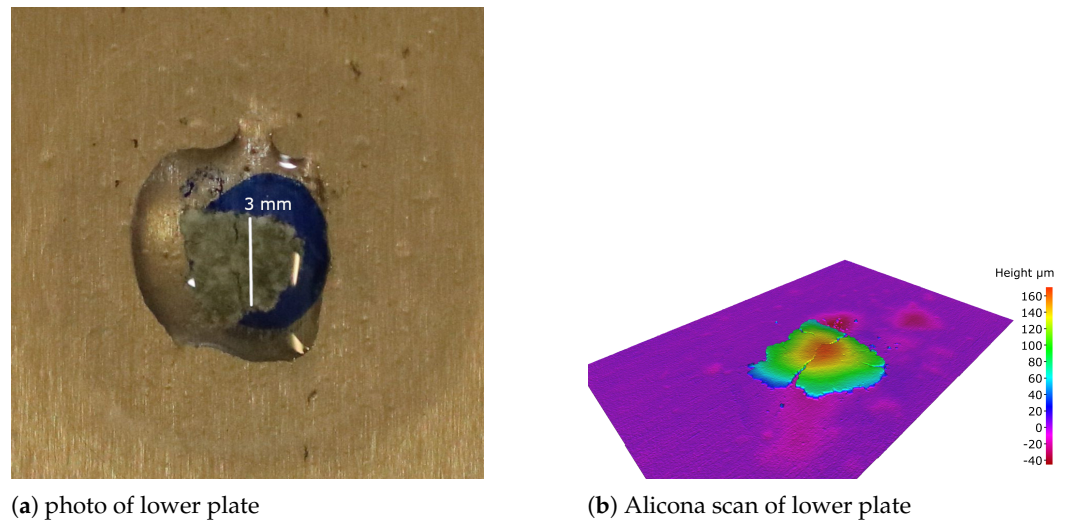


**Figure 16.** Example result for high load testing of AT sand under wet conditions.

To further investigate the formed clusters' surface, SEM images were taken from solidified fragments of GB and AT sand. This was an attempt to see if the larger fragments/clusters were composed of connected smaller fragments. Figure 17 shows the obtained SEM images of one larger solidified cluster and a zoom in of both GB and AT sand. The zoom in of the GB sand cluster contains a crack, which might have occurred during the loading test or during preparation of the sample for the SEM imaging. The solidified sand looks like a solid material, no composition of smaller fragments can be seen on the surface or within the cracked area. The same holds true for the AT sand, where the zoom in shows areas of smooth surface alternating with areas of higher surface structure.

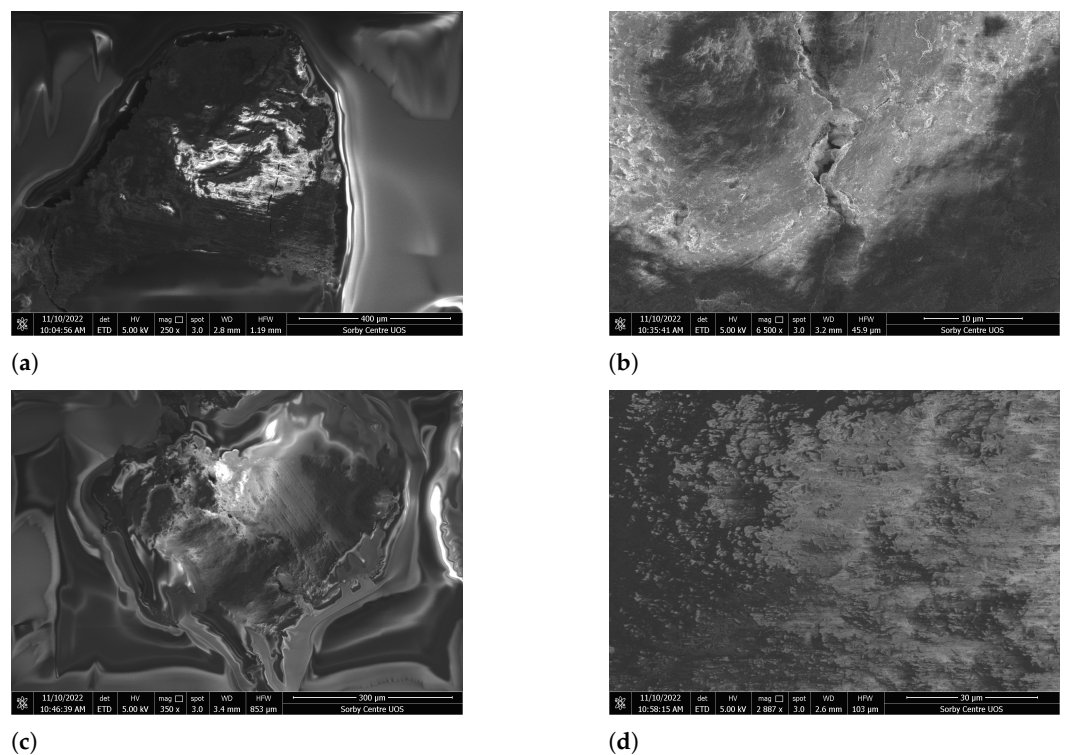


**Figure 17.** SEM images of solidified clusters of GB and AT sand after conducting high load tests. (a) GB sand: large cluster fragment surrounded by glue; (b) GB sand: zoom in; (c) AT sand: large cluster fragment surrounded by glue; (d) AT sand: zoom in.

#### 4. Discussion

This study gives new insights in the crushing behaviour of sand grains with the application of sanded wheel–rail contacts. Sand grains and their fragments are repeatedly crushed during roll-over. Obviously, adhesion can be improved only by those fragments which stay in the contact zone, in contrast to those which are expelled during fracture. The amount of these fragments in the contact zone depends on the type of sand, which differ in grain size, and the contact conditions (dry vs. wet conditions). Even in the first breakage tests clear differences were seen in the spreading behaviour of fragments of GB and AT sand under dry and wet conditions, see Figure 8.

Under realistic service conditions, wheel–rail rolling contact is a rolling-sliding state involving creepage. In this study, creepage is not considered. In order to separate the different effects the focus is on pure vertical loading of the sand grains. It is assumed that there is little influence on the initial breakage by creepage occurring in parallel to the vertical loading.

When a sand grain is entrained in the wheel–rail contact, it will be crushed, with its fragments spreading out. In the conducted initial breakage tests, differences in the spreading behaviour for both types of sand and dry or wet contact conditions were seen. This breakage-spreading process happens repeatedly for those fragments which stay in the running band. Under the extremely high loads in the wheel–rail contact, the sand fragments in the contact zone form clusters, as it was seen in the conducted high load crushing tests. In these tests, the amount of fragments/cluster size depend again on the type of sand, which differ in grain size, and the contact condition, see Figures 13–16. Under the applied high load, the clusters reached a typical thickness in the order of 100 to a 220  $\mu\text{m}$ . Under such extreme loading conditions these sand clusters seem to behave like a solid with certain elasto-plastic material behaviour. For example, Figure 15 shows a cluster with cracks growing from the border towards the centre, which would be a result expected from crushing a solid elasto-plastic material. The clusters' solid-like behaviour is also confirmed by the SEM images shown in Figure 17 revealing that the clusters are obviously not a loose conglomerate of smaller fragments.

It is expected that these solid-like sand clusters are encapsulated between wheel and rail surfaces. The huge local stresses in their vicinity are likely to cause plastic deformations and thus change the surface roughness of wheel and rail. This assumption was indirectly confirmed by the high load crushing tests. For example, in the Alicona scans in Figures 15 and 16 there are indentations around the clusters with a depth in the order of 20–40  $\mu\text{m}$ . These indentations stem from previous tests, as the same upper and lower plate made of hardened steel were used for all tests.

To summarise, this work supports the assumption that the positive effect of sand on the friction in the wheel–rail interface under low adhesion conditions comes about as follows. Dependent on the type of sand and the contact condition, in sanded wheel–rail contacts sand clusters of different size will form. These clusters will be encapsulated between wheel and rail surface, they become plastically deformed and will also plastically indent into the wheel and rail surfaces causing some kind of form-closure effects. Under slip conditions, the relative motion between wheel and rail could occur (i) at the border between the sand cluster and the wheel and rail surfaces, (ii) in shear bands within the sand cluster or (iii) a combination of both.

The described behaviour and the results from the breakage tests can be related to some extent to the sand's influence on the adhesion coefficient in HPT tests, see Figure 2. Under dry conditions, GB sand leaves the AC mostly unchanged, while a clear reduction in the AC can be seen for AT sand. Under wet conditions, both types of sand increase the measured AC, while this effect is more pronounced for GB than for AT sand. For AT sand the ACs obtained under dry and wet conditions are similar—with the AC under dry conditions being slightly higher than that obtained under wet conditions.

One hypothesis to explain these measured ACs in the HPT tests is: If there is enough sand in the contact, then the AC will be determined by the shearing behaviour of the formed sand clusters.

For GB sand under dry conditions, it seems likely that large part of the initial mass of GB sand is expelled from the HPT test. This is supported by the initial crushing tests, see Figure 8a, and also by most results of the high loading tests, see Figure 13. If only little amounts of sand fragments are present during the HPT tests, this will explain why the measured AC for GB sand is close to the unsanded case.

For GB sand under wet conditions, the conducted high loading tests showed large clusters of sand formed, Figure 15, which will increase the AC in the way described above.

For AT sand, dry and wet contact conditions gave similar results: the initial crushing tests showed that nearly all fragments stayed in the contact zone, see Figure 8b, and in the high load tests large clusters formed, see Figures 14 and 16. It seems likely that the shearing behaviour of these clusters determines the measured AC values and thus give similar results both under dry and wet conditions. Compared to the unsanded case, under dry conditions the AT sand can be thought as dry lubrication, reducing the AC. In contrast, under wet conditions it increases the AC compared to the unsanded case.

It is an open question, why under wet conditions GB sand increases the AC more than AT sand does. On the one hand, it could be related to GB sand's larger initial grain size which leads to larger clusters in the high loading tests. On the other hand, also other properties of the sand types can be expected to influence the measured AC.

Based on the results of this study future tests are planned: small scale shear-box experiments should give information about the shearing behaviour of solidified clusters. This is important for the physics-based models to be developed.

**Author Contributions:** Conceptualization, B.S., W.A.S., R.L. and K.S.; methodology, B.S., W.A.S., R.L. and K.S.; formal analysis, B.S.; investigation, W.A.S.; resources, R.L.; data curation, B.S. and W.A.S.; writing—original draft preparation, B.S.; writing—review and editing, B.S., W.A.S., R.L. and K.S.; visualization, B.S. and W.A.S.; supervision, K.S. and R.L.; project administration, B.S.; funding acquisition, B.S. All authors have read and agreed to the published version of the manuscript.

**Funding:** This research was funded in whole, or in part, by the Austrian Science Fund (FWF) project P 34273: DEM modelling of adhesion in sanded wheel–rail contacts. For the purpose of open access, the author has applied a CC BY public copyright licence to any Author Accepted Manuscript version arising from this submission. The publication was written at Virtual Vehicle Research GmbH in Graz and partially funded by the COMET K2—Competence Centers for Excellent Technologies Programme of the Federal Ministry for Climate Action (bmk), the Federal Ministry for Digital and Economic Affairs (bmdw), the Austrian Research Promotion Agency (FFG), the Province of Styria, and the Styrian Business Promotion Agency (SFG).

**Data Availability Statement:** The data set generated and analysed during the current study is openly available in the zenodo.org repository: Suhr, Bettina, Six, Klaus, Skipper, William, & Lewis, Roger. (2023). Single grain crushing tests on two sand types used for wheel-rail sanding [Data set]. Zenodo. DOI [10.5281/zenodo.7547518](https://doi.org/10.5281/zenodo.7547518).

**Conflicts of Interest:** The authors declare no conflict of interest.

## Abbreviations

The following abbreviations are used in this manuscript:

3BL	third body layer
AC	adhesion coefficient
HPT	high pressure torsion
SEM	Scanning Electron Microscope
UMT	universal mechanical tester



## References

1. Six, K.; Meierhofer, A.; Trummer, G.; Bernsteiner, C.; Marte, C.; Müller, G.; Luber, B.; Dietmaier, P.; Rosenberger, M. Plasticity in wheel-rail contact and its implications on vehicle-track interaction. *Proc. Inst. Mech. Eng. Part F J. Rail Rapid Transit* **2017**, *231*, 558–569. [\[CrossRef\]](#)
2. Eden, H.C.; Garnham, J.E.; Davis, C.L. Influential microstructural changes on rolling contact fatigue crack initiation in pearlitic rail steels. *Mater. Sci. Technol.* **2005**, *21*, 623–629. [\[CrossRef\]](#)
3. Alwahdi, F.; Kapoor, A.; Franklin, F. Subsurface microstructural analysis and mechanical properties of pearlitic rail steels in service. *Wear* **2013**, *302*, 1453–1460. [\[CrossRef\]](#)
4. Garnham, J.; Davis, C. Very early stage rolling contact fatigue crack growth in pearlitic rail steels. *Wear* **2011**, *271*, 100–112. [\[CrossRef\]](#)
5. Trummer, G.; Marte, C.; Scheriau, S.; Dietmaier, P.; Sommitsch, C.; Six, K. Modeling wear and rolling contact fatigue: Parametric study and experimental results. *Wear* **2016**, *366–367*, 71–77. [\[CrossRef\]](#)
6. Trummer, G.; Six, K.; Marte, C.; Dietmaier, P.; Sommitsch, C. An approximate model to predict near-surface ratcheting of rails under high traction coefficients. *Wear* **2014**, *314*, 28–35. [\[CrossRef\]](#)
7. Trummer, G.; Six, K.; Marte, C.; Meierhofer, A.; Sommitsch, C. Automated measurement of near-surface plastic shear strain. In Proceedings of the 2nd International Conference on Railway Technology: Research, Development and Maintenance, Ajaccio, Corsica, France, 8 April–11 April 2014; p. 104.
8. Polach, O. Creep forces in simulations of traction vehicles running on adhesion limit. *Wear* **2005**, *258*, 992–1000. [\[CrossRef\]](#)
9. Six, K.; Meierhofer, A.; Müller, G.; Dietmaier, P. Physical processes in wheel-rail contact and its implications on vehicle-track interaction. *Veh. Syst. Dyn. Int. J. Veh. Mech. Mobil.* **2015**, *53*, 635–650. [\[CrossRef\]](#)
10. Meierhofer, A.; Hardwick, C.; Lewis, R.; Six, K.; Dietmaier, P. Third body layer—experimental results and a model describing its influence on the traction coefficient. *Wear* **2014**, *314*, 148–154. [\[CrossRef\]](#)
11. Lewis, R.; Dwyer-Joyce, R.; Lewis, S.; Hardwick, C.; Gallardo-Hernandez, E. Tribology of the Wheel-Rail Contact: The Effect of Third Body Materials. *Int. J. Railw. Technol.* **2012**, *1*, 167–194. [\[CrossRef\]](#)
12. Descartes, S.; Desrayaud, C.; Niccolini, E.; Berthier, Y. Presence and role of the third body in a wheel-rail contact. *Wear* **2005**, *258*, 1081–1090. [\[CrossRef\]](#)
13. Niccolini, E.; Berthier, Y. Wheel-rail adhesion: Laboratory study of “natural” third body role on locomotives wheels and rails. *Wear* **2005**, *258*, 1172–1178. [\[CrossRef\]](#)
14. Buckley-Johnstone, L.; Trummer, G.; Voltr, P.; Meierhofer, A.; Six, K.; Fletcher, D.; Lewis, R. Assessing the impact of small amounts of water and iron oxides on adhesion in the wheel/rail interface using High Pressure Torsion testing. *Tribol. Int.* **2019**, *135*, 55–64. [\[CrossRef\]](#)
15. White, B.; Nilsson, R.; Olofsson, U.; Arnall, A.; Evans, M.; Armitage, T.; Fisk, J.; Fletcher, D.; Lewis, R. Effect of the presence of moisture at the wheel-rail interface during dew and damp conditions. *Proc. Inst. Mech. Eng. Part F J. Rail Rapid Transit* **2018**, *232*, 979–989. [\[CrossRef\]](#)
16. White, B.; Lewis, R. Simulation and understanding the wet-rail phenomenon using twin disc testing. *Tribol. Int.* **2019**, *136*, 475–486. [\[CrossRef\]](#)
17. Trummer, G.; Buckley-Johnstone, L.; Voltr, P.; Meierhofer, A.; Lewis, R.; Six, K. Wheel-rail creep force model for predicting water induced low adhesion phenomena. *Tribol. Int.* **2017**, *109*, 409–415. [\[CrossRef\]](#)
18. Lewis, R.; Dwyer-Joyce, R.; Lewis, J. Disc machine study of contact isolation during railway track sanding. *Proc. Inst. Mech. Eng. Part F J. Rail Rapid Transit* **2003**, *217*, 11–24. [\[CrossRef\]](#)
19. Lewis, R.; Dwyer-Joyce, R. Wear at the wheel/rail interface when sanding is used to increase adhesion. *Proc. Inst. Mech. Eng. Part F J. Rail Rapid Transit* **2006**, *220*, 29–41. [\[CrossRef\]](#)
20. Skipper, W.A.; Chalisey, A.; Lewis, R. A review of railway sanding system research: Adhesion restoration and leaf layer removal. *Tribol.-Mater. Surf. Interfaces* **2018**, *12*, 237–251. [\[CrossRef\]](#)
21. Skipper, W.; Chalisey, A.; R., L. A Review of Railway Sanding System Research: Wheel/Rail Isolation, Damage, and Particle Application. *Proc. Inst. Mech. Eng. Part F J. Rail Rapid Transit* **2019**, *234*, 567–583. [\[CrossRef\]](#)
22. Arias-Cuevas, O.; Li, Z.; Lewis, R. Investigating the Lubricity and Electrical Insulation Caused by Sanding in Dry Wheel-Rail Contacts. *Tribol. Lett.* **2010**, *37*, 623–635. [\[CrossRef\]](#)
23. Wang, W.; Zhang, H.; Wang, H.; Liu, Q.; Zhu, M. Study on the adhesion behavior of wheel/rail under oil, water and sanding conditions. *Wear* **2011**, *271*, 2693–2698. [\[CrossRef\]](#)
24. Wang, W.; Liu, T.; Wang, H.; Liu, Q.; Zhu, M.; Jin, X. Influence of friction modifiers on improving adhesion and surface damage of wheel/rail under low adhesion conditions. *Tribol. Int.* **2014**, *75*, 16–23. [\[CrossRef\]](#)
25. Huang, W.; Cao, X.; Wen, Z.; Wang, W.; Liu, Q.; Zhu, M.; Jin, X. A Subscale Experimental Investigation on the Influence of Sanding on Adhesion and Rolling Contact Fatigue of Wheel/Rail Under Water Condition. *J. Tribol.* **2017**, *139*, 011401. [\[CrossRef\]](#)
26. Lewis, S.R.; Riley, S.; Fletcher, D.I.; Lewis, R. Optimisation of a Railway Sanding System, Part 2: Adhesion Tests. In Proceedings of the 10th International Conference on Contact Mechanics (CM2015), Colorado Springs, CO, USA, 30 August–3 September 2015.
27. Skipper, W.; Nadimi, S.; Chalisey, A.; Lewis, R. Particle characterisation of rail sands for understanding tribological behaviour. *Wear* **2019**, 432–433, 202960. [\[CrossRef\]](#)

28. Skipper, W. Sand Particle Entrainment and its Effects on the Wheel/Rail Interface. Ph.D. Thesis, University of Sheffield, Sheffield, UK, 2021.
29. Vollebregt, E.; Six, K.; Polach, O. Challenges and progress in the understanding and modelling of the wheel–rail creep forces. *Veh. Syst. Dyn.* **2021**, *59*, 1026–1068. [\[CrossRef\]](#)
30. Carter, F.W. On the Action of a Locomotive Driving Wheel. *Proc. R. Soc. Lond. Ser. A Contain. Pap. Math. Phys. Character* **1926**, *112*, 151–157. [\[CrossRef\]](#)
31. Fromm, H. Berechnung des Schlupfes beim Rollen deformierbarer Scheiben. *Z. Angew. Math. Mech.* **1927**, *7*, 27–58. [\[CrossRef\]](#)
32. Johnson, K. The effect of a tangential contact force upon the rolling motion of an elastic sphere upon a plane. *J. Appl. Mech.* **1958**, *25*, 339–346. [\[CrossRef\]](#)
33. Johnson, K. The effect of spin upon the rolling motion of an elastic sphere upon a plane. *J. Appl. Mech.* **1958**, *25*, 332–338. [\[CrossRef\]](#)
34. Kalker, J. The computation of three-dimensional rolling contact with dry friction. *Int. J. Numer. Methods Eng.* **1979**, *14*, 1293–1307. [\[CrossRef\]](#)
35. Kalker, J.J. On the Rolling Contact of Two Elastic Bodies in the Presence of Dry Friction. Ph.D. Thesis, Delft University of Technology, Delft, The Netherlands, 1967.
36. Kalker, J.J. Simplified Theory of Rolling Contact. *Delft Progr. Rep. Ser. C Mech. Aeronaut. Eng. Shipbuild.* **1973**, *1*, 1–10.
37. Kalker, J.J. A Fast Algorithm for the Simplified Theory of Rolling Contact. *Veh. Syst. Dyn.* **1982**, *11*, 1–13. [\[CrossRef\]](#)
38. Kalker, J.J. *Three-Dimensional Elastic Bodies in Rolling Contact*; Kluwer Academic Press: Dordrecht, The Netherlands, 1990; ISBN 978-94-015-7889-9.
39. Knothe, K. History of wheel/rail contact mechanics: From Redtenbacher to Kalker. *Veh. Syst. Dyn.* **2008**, *46*, 9–26. [\[CrossRef\]](#)
40. Poritsky, H. Stresses and deflections of cylindrical bodies in contact with application to contact of gears and of locomotive wheels. *J. Appl. Mech.-Trans. ASME* **1950**, *17*, 191–201. [\[CrossRef\]](#)
41. Meymand, S.Z.; Keylin, A.; Ahmadian, M. A survey of wheel-rail contact models for rail vehicles. *Veh. Syst. Dyn.* **2016**, *54*, 386–428. [\[CrossRef\]](#)
42. Vollebregt, E.A.H.; van der Wekken, C.D. *Advanced Modeling of Wheel–Rail Friction Phenomena*; Technical Report TR19-11; VORtech: Irwindale, CA, USA, 2019.
43. Van der Wekken, C.; Vollebregt, E. Local plasticity modelling and its influence on wheel-rail friction. In Proceedings of the Proceedings of the 11th International Conference on Contact Mechanics and Wear of Rail/Wheel Systems, Delft, The Netherlands, 24–27 September 2018; pp. 1013–1018.
44. Allen, T. *Particle Size Measurement*, 3rd ed.; Chapman & Hall: London, UK, 1981.
45. BS 1377-2:1990; Methods of Test for Soils for Civil Engineering Purposes: Part 2: Classification Tests. British Standards Institute: London, UK, 1990.
46. Schindelin, J.; Arganda-Carreras, I.; Frise, E.; Kaynig, V.; Longair, M.; Pietzsch, T.; Preibisch, S.; Rueden, C.; Saalfeld, S.; Schmid, B.; et al. Fiji: An open-source platform for biological-image analysis. *Nat. Methods* **2012**, *9*, 676–682. [\[CrossRef\]](#)
47. The GIMP Development Team. GIMP Version 2.10.22. Available online: <https://www.gimp.org> (accessed on 15 December 2022).
48. Bernsteiner, C.; Müller, G.; Meierhofer, A.; Six, K.; Künstner, D.; Dietmaier, P. Development of white etching layers on rails: simulations and experiments. *Wear* **2016**, *366–367*, 116–122. [\[CrossRef\]](#)
49. McDowell, G.R.; Bolton, M.D. On the micromechanics of crushable aggregates. *Géotechnique* **1998**, *48*, 667–679. [\[CrossRef\]](#)
50. Lim, W.; McDowell, G.; Collop, A. The application of Weibull statistics to the strength of railway ballast. *Granul. Matter* **2004**, *6*, 229–237. [\[CrossRef\]](#)
51. Laufer, I. Grain crushing and high-pressure oedometer tests simulated with the discrete element method. *Granul. Matter* **2015**, *17*, 389–412. [\[CrossRef\]](#)
52. Weibull, W. A statistical distribution of wide applicability. *J. Appl. Mech.* **1951**, *18*, 293–297. [\[CrossRef\]](#)

**Disclaimer/Publisher’s Note:** The statements, opinions and data contained in all publications are solely those of the individual author(s) and contributor(s) and not of MDPI and/or the editor(s). MDPI and/or the editor(s) disclaim responsibility for any injury to people or property resulting from any ideas, methods, instructions or products referred to in the content.